BMES BIOMEDICAL ENGINEERING SOCIETY

CrossMark

Real-Time Bioimpedance-Based Biopsy Needle Can Identify Tissue Type with High Spatial Accuracy

SANNA HALONEN [iD],[1,2] JUHO KARI,[1] PETRI AHONEN,[1] KAI KRONSTRÖM,[1] and JARI HYTTINEN[2]

[1]R&D Department, Injeq Ltd, Hermiankatu 22, 33720 Tampere, Finland; and [2]BioMediTech Institute and Faculty of Biomedical Sciences and Engineering, Tampere University of Technology, Korkeakoulunkatu 10, Tampere, Finland

Associate Editor Sean S. Kohles oversaw the review of this article.

Abstract—Histological analysis is meaningful in diagnosis only if the targeted tissue is obtained in the biopsy. Often, physicians have to take a tissue sample without accurate information about the location of the instrument tip. A novel biopsy needle with bioimpedance-based tissue identification has been developed to provide data for the automatic classification of the tissue type at the tip of the needle. The aim of this study was to examine the resolution of this identification method and to assess how tissue heterogeneities affect the measurement and tissue classification. Finite element method simulations of bioimpedance measurements were performed using a 3D model. *In vivo* data of a porcine model were gathered with a moving needle from fat, muscle, blood, liver, and spleen, and a tissue classifier was created and tested based on the gathered data. Simulations showed that very small targets were detectable, and targets of $2 \times 2 \times 2$ mm^3 and larger were correctly measurable. Based on the *in vivo* data, the performance of the tissue classifier was high. The total accuracy of classifying different tissues was approximately 94%. Our results indicate that local bioimpedance-based tissue classification is feasible *in vivo*, and thus the method provides high potential to improve clinical biopsy procedures.

Keywords—Tissue classification, *In vivo*, Animal study, Simulations, Tissue properties, Liver, Hepatic tissue.

INTRODUCTION

Biopsies play a key role in the treatment of diseases, such as cancer. Tissue samples, however, only represent a small proportion of the organ, and therefore the accurate selection of the sampling site is of the utmost importance. Furthermore, unrepresentative tissue samples can lead to misdiagnosis and delays in treatments. With a conventional biopsy, for example, the

false-negative rate for prostate cancer can be as high as 38%.[26]

Tumorous tissue is often characterized as having a unique or unordered structure and abnormal vascularization. In large tumors, the interior is often necrotic. Because the histology changes, the electrical properties of the tissue most likely also change. In fact, multiple studies indicate that bioimpedance can differentiate tumorous tissue from benign tissue. For example, *ex vivo* prostate cancer[10,20,21] and hepatic tumors[6,19,23] have been studied with promising results.

Measurement probe embedded directly in a medical instrument could provide a practical method for tissue detection. Bioimpedance-measuring needles have been studied in animal and *ex vivo* studies for general tissue discrimination purposes,[12,27] for detecting transcutaneous kidney access,[11] for detecting nerve tissue,[13] and for measuring muscle properties.[18] In addition, Mishra *et al.*[21] investigated the use of a biopsy needle for prostate cancer using *ex vivo* samples. They reported a performance of approximately 75% in discriminating cancerous and non-cancerous tissue. However, they also reported a weakness with the method in that it not only measures the sampled tissue but also the surrounding tissue. In fact, using their configuration, only 5% of the sensitivity distribution was in the sampled tissue volume according to our resistive finite element method (FEM) simulation.[9]

Many instruments used in animal or *ex vivo* impedance studies do not fulfill the requirements for clinical use because the probe is unsuitable for use in humans (large size, toxic, or materials not sterilizable), the probe is not suitable for manufacturing, the instrumentation is not suitable for use in humans (electrical safety regulations), or the measurement de-

Address correspondence to Sanna Halonen, R&D Department, Injeq Ltd, Hermiankatu 22, 33720 Tampere, Finland. Electronic mail: sanna.halonen@injeq.com

vice is impractical for medical use (slow measurement, complex user-interface).

A thin hypodermic needle with integrated bioimpedance measurement electrodes can enable easy integration into the clinical workflow and spatial accuracy of the measurement.[14] Such a needle setup has previously been used successfully in clinical intra-articular injections[8] and spinal anesthesia.[7] Similar measurement principles have also been adapted to biopsy needles, and a 14G prototype has been tested in animals.[9] The biopsy needle discussed here was created using a non-centric configuration with the aim of concentrating the measurement sensitivity distribution at the very tip of the needle. Our initial simulations in purely resistive homogenous media showed a very local sensitivity distribution. With quasi-static FEM, approximately 98% of the distribution was in the volume in front of the needle facet, meaning that essentially everything that is measured would also be sampled.[9]

The prototype biopsy needle has now been further developed for clinical use. The needle has a size and tip geometry equal to those used clinically, and it is made from biocompatible and sterilizable materials. Furthermore, the measurement device is simple to use and fulfills safety regulations. In clinical use, the needle should enable the detection of local tissue targets, and the classification of the tissue should be ensured despite the inevitable artifacts from movements of the needle and tissue heterogeneity. A final aim is to create a useful tool to help physicians guide the biopsy procedure. Such a tool would enhance biopsy quality and make the procedure easier by providing precise needle location information on whether the selected target has been reached or not.

The aim of this study is to assess the properties and performance of the novel Injeq IQ-Biopsy needle. In the study, the spatial measurement properties of the needle for identifying targets and the tissue discrimination ability targeted for real-time tissue identification using liver biopsy as an example were investigated. To do this, we used FEM simulations of a penetrating needle to test its capability to detect tissue boundaries and small, variably sized tissue targets in the path of the penetrating needle or close to it. In addition to simulations, the biopsy device was also tested *in vivo* in a porcine model with 21 punctures in five tissue type*s* to test whether it is possible to identify macroscopically different tissues with highly local measurement, and what kind of classification performance can be achieved from *in vivo* data. Classifier analysis provided a basis for creating initial classification parameters before clinical studies. To the best of our knowledge, this is the first time that a clinically suitable biopsy system has been used in bioimpedance-based local

in vivo tissue discrimination and its performance values reported. Moreover, the results are generally applicable to bioimpedance tissue measurement and classification.

MATERIALS AND METHODS

Measurement System

Measurements were performed using an Injeq IQ-Biopsy system that comprised an IQ-Biopsy Needle, IQ-Biopsy instrument, coaxial cable, and the Injeq BZ-301 impedance analyzer with modified parameters (Fig. 1). During the study, the system was still in the research and development phase and was not commercially available. The biopsy needles had a similar geometry and mechanical working principle to the conventional Bard® Magnum® core-biopsy needle, but when connected to the measurement device, the IQ-Biopsy needle could measure and record bioimpedance spectra.

The biopsy needles were core-type biopsy needles having a size of 18G (outer diameter 1.27 mm) and comprised two nested stainless-steel needles. The needle is punctured in the loaded state, and when the target is reached, the biopsy instrument fires the two nested needles forward for tissue collection. The inner needle, with a sampling notch, proceeds first, and the outer needle follows immediately after, cutting and trapping the sample into the notch.

In the IQ-Biopsy Needle, the inner needle also has an electrode wire inside it that is insulated from the needle cannula. Bioimpedance measurement was performed at multiple measurement frequencies between the electrode wire and the inner needle cannula, as
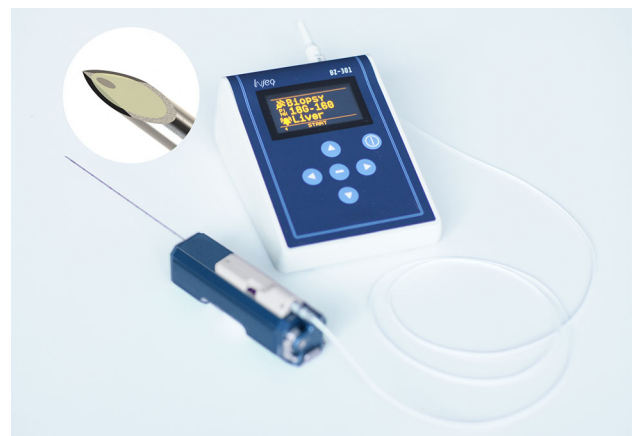
FIGURE 1. The Injeq BZ-301 measurement device and Injeq IQ-Biopsy system. The enlargement of the needle tip shows the electrode wire inside the inner needle. The image is published with kind permission of Injeq Ltd, which holds the copyright.

described in Refs. 7, 9, and 14. This configuration enabled the measurement from the very tip of the inner needle. The electrode wire was placed eccentrically to the other edge of the inner needle in such a way that the tip of the electrode wire was closer to the tip of the needle than where it would be in a centric configuration (Fig. 1). Hence, the sensitivity distribution was drawn even further to the very tip of the needle.

In the needle, the same electrodes were used for both feeding the excitation signal and for measurement. Due to this bipolar measurement principle, electrode interface impedance (EII) affected the measurement values. The effect was strongest at low measurement frequencies (see the measured impedance spectra of the needle obtained in saline solution in Fig. 2). It is, however, also possible that EII is tissue-type dependent due to various electrolytic conditions, and this would make EII estimation uncertain.

The sampling rate of the bioimpedance analyzer was 200 Hz. Fast measurement was achieved by using an excitation signal that was a customized sequence of binary pulses, with power focused on the desired frequencies as in Ref. 2. Thus, one excitation signal provided the information of all the desired measurement frequencies simultaneously, and multiple sweeps were not needed.

The presynthesized multifrequency binary excitation signal was transformed to analog output using an enhanced pulse-width modulator.[2] The excitation signal comprises sequences of binary values that create a series of rectangular pulse signals. By modulating the length, number, and repetition of these pulses, the frequency content of the injected signal can be controlled. By applying this spectrally designed binary excitation, the voltage and current were measured from the device's analog inputs. The complex transfer function of the measured impedance was calculated *via*

Discrete Fourier Transform of the voltage and current signals. The actual impedance response was calculated using convolution.

The data processing part of the device uses the DSP efficient DFT-algorithm to extract real and imaginary parts of the complex value from the measured voltage and current at 15 frequency-points between 1 and 350 kHz. These complex values were then passed to the classifier unit where input phase and module data were converted to feature data. The tissue classification is made based on feature data.

The measurement device was optimized for safe, fast, real-time measurement rather than absolute accuracy. The binary excitation approach causes aliasing to the impedance value.[2] In addition, because the device has doubled components and electronics designed to ensure safe operation and to fulfill electrical safety regulation IEC60601, the measurements were affected. Measurement device error was estimated using multiple combinations of resistors and capacitors in parallel. Component combinations do not provide spectra that represent tissue over all frequencies, and therefore the RC error model provided only a rough estimation of the measurement error on the specified frequency. The stray capacitance from the cabling, the biopsy instrument, and the needle was approximately 160 pF. Its effect was estimated and compensated using the open compensation method,[22] where the capacitance of the cable and instrument Z_{cabling} is measured first without load. The impedance of the target Z_{target} is then obtained by subtracting the open impedance including the stay capacitance from the measured total impedance Z_{measured}.

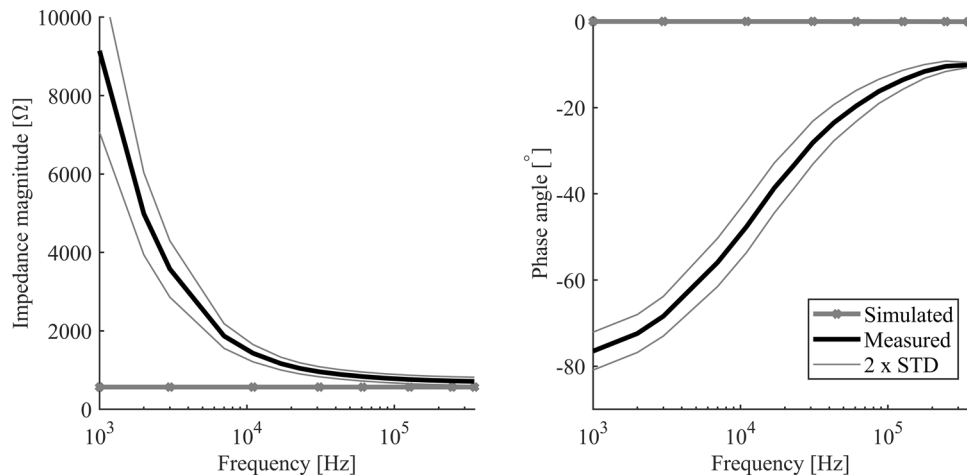$$\frac{1}{Z_{\text{target}}} = \frac{1}{Z_{\text{measured}}} - \frac{1}{Z_{\text{cabling}}}$$

FIGURE 2. Frequency spectra of measured and simulated impedance of 0.9% saline.

For tissue discrimination purposes, the absolute impedance value is not critical, but high repeatability plays a crucial role. The repeatability of the measurement device was high. Depending on the measurement frequency and measurement target, impedance magnitude differences in repeated RC measurements were on the level of 0.5%.

Simulations

The measurement properties of the IQ-Biopsy were simulated using 3D FEM (COMSOL Multiphysics®v.5.2.a, Stockholm), including both the resistive and reactive properties of the material. The outer needle, inner needle, and electrode wire diameters were 1.3, 1.02, and 0.2 mm, respectively, and corresponded to the geometry of the 18G IQ-Biopsy. The main bevel angle of the needle tip was 17°. The outer boundaries of the needle were set as a ground potential, and the tip of the electrode wire was set as a terminal. A nominal current of 1 A was introduced through the terminal into the system. All outer boundaries of the simulated system were insulated. Extra-fine physics-controlled tetrahedral mesh was used. The simulated systems had approximately 520,000 tetrahedral mesh elements, 20,000 triangular elements, 1000 edge elements, and 31 vertex elements. The element size ranged from 0.075 to 1.75 mm. The mesh elements were smallest nearest the needle electrodes. All material properties were set to be isotropic. A stationary linear solver with the iterative biconjugate gradient stabilized method were used to solve the complex impedance at 127 kHz.

The significant volume for the needle measurement was evaluated using the sensitivity distribution S of the impedance measurement, defined as

$$S = J_{res} \cdot J_{current}$$

where J_{res} and $J_{current}$ are the current density field of the reciprocal current between the voltage measurement electrodes and the feeding current electrodes, respectively.[5] In our configuration, the same electrode pair was used for current feeding and measurement, and therefore, the equation has the simplified form:

$$S = |J_{current}|^2$$

The resulting impedance Z can be calculated from the sensitivity distribution, conductivity σ, and the permittivity ε of the measured volume as an integration over the volume V[5]

$$Z = \int_V \frac{1}{\sigma + j\omega\varepsilon} S dV$$

Thus, the sensitivity distribution describes the spatial sampling properties of the measurement arrangement when there is no change in conductivity or in permittivity over the volume. Visualization of the computed S provided a way to assess impedance measurement arrangements.[15] The technique is widely used for whole body impedance cardiography and for microelectrodes in cell culture.[3,15–17] We visualized the sensitivity distribution of the needle system in homogeneous media. However, the impedance values during the penetrations of different targets were calculated directly from the current and voltages on the simulated electrodes.

Multiple volume conductor cases were simulated using a $50 \times 50 \times 50$ mm³ cube (Fig. 3). The needle in the cube was defined using boundary conditions, so that no simulation of the interior of the needle was needed (defined as a vacuum). The following types of simulation were made: (1) needle in a homogeneous block, (2) needle penetration to another tissue, (3) needle penetration through a membrane, (4) needle
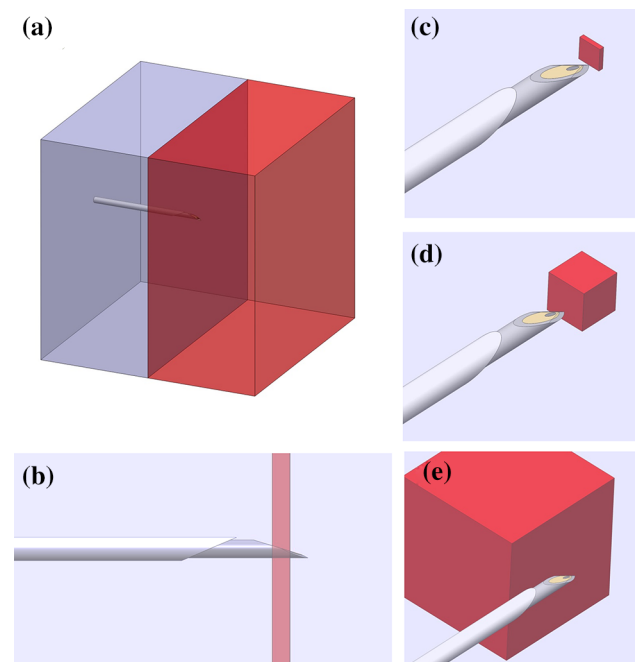
FIGURE 3. 3D finite element method simulation geometries: (a) the needle in the $50 \times 50 \times 50$ mm³ cube where there is tissue change. (b)–(e) are zoomed to the target and needle tip inside the cube. The surrounding tissue is in blue and the target tissue is in red. (b) shows a 1 mm thick membrane, (c) shows a $0.2 \times 1 \times 1$ mm³ heterogeneity in front of the needle, (d) shows a $2 \times 2 \times 2$ mm³ heterogeneity, and (e) shows a heterogeneity of $10 \times 10 \times 10$ mm³ next to the needle penetration route. In (e) the heterogeneity touches the outer needle surface, but is not on the needle penetration route. This simulation has also been repeated with a different needle facet direction compared to the heterogeneity.

penetration through a small heterogeneity and (5) needle below, above, or beside a heterogeneity. The membranes in the simulations represented any thin anatomical structure in the body, such as endothelia or epithelia layers lining the tissue structures or inter tissue layers in the interior ligaments of the liver.

Tissue change was simulated using homogeneous blocks. A tissue boundary was placed in the middle of the block, perpendicular to the longitudinal axis of the needle. The needle was moved along its longitudinal axis from one tissue to another step-by-step. Subsequently, the impedance signal was calculated for each step from the voltage on the surface of the inner electrode using Ohm's law. The penetration was perpendicular to the tissue interface. The aim was to show how different kinds of heterogeneity in tissues are seen in the impedance signal and to determine whether there are differences in resolution when measuring better or worse conducting materials. The surrounding tissue had a conductivity of 0.1 S/m and a relative permittivity of 5000. Compared with the surrounding tissue, the other tissue had higher and lower conductivities and relative permittivities, with conductivity values of 0.01, 0.05, 0.075, 0.1, 0.133, 0.2, and 1 S/m and relative permittivity values of 1, 1000, 5000, 10,000, and 100,000. All 35 combinations were simulated. These material values were selected to cover the typical tissue properties at 127 kHz and beyond. For example, fat is a low conductive material with a conductivity of 0.02 to 0.05 S/m and relative permittivity of 20 to 80,[4] while blood is a high conductive material, with a conductivity of about 0.7 S/m and a relative permittivity of approximately 10,000.[29]

Membrane and small-heterogeneity penetrations were simulated using the same conductivity and permittivity values. The thickness of the simulated membrane was 1 mm, and the sizes of the heterogeneities were $0.2 \times 1 \times 1$, $0.5 \times 1 \times 1$, $1 \times 1 \times 1$, and $2 \times 2 \times 2$ mm^3, of which the first dimension was in the direction of needle penetration.

To estimate how much the heterogeneities next to the needle penetration route affected the impedance, simulations were performed with a block of $10 \times 10 \times 10$ mm^3 above, below, and next to the asymmetric biopsy needle. The heterogeneity was placed so that it touched the surface of the outer needle but was not in front of the needle facet. Thus, if the needle had been fired, the heterogeneity would not have been sampled.

When penetrating new tissue or a heterogeneity, the change in impedance was considered to be significant and detectable if it was over 5% of the impedance magnitude of the surrounding tissue or over 2° in phase angle. In addition to detectability, we also analyzed when the new tissue or heterogeneity was correctly measurable. The heterogeneity was considered to be correctly measurable if the obtained impedance from the heterogeneity differed by less than 5% from the impedance magnitude and less than 2° in phase angle of the pure heterogeneity.

Animal Study

In vivo porcine tissues were measured with the IQ-Biopsy system. The pig (male, about 45 kg) was anesthetized during the study, and an experienced veterinarian monitored the study. The study was authorized by the Ethics Committee of the Southern Finland Regional State Administrative Agency (ESA-VI/4389/04.10.07/2015).

Two types of data were gathered: (1) ultrasound-guided liver biopsies and (2) multiple visually controlled punctures into adipose tissue, muscle, liver, spleen, and blood with seven biopsy needles. The ultrasound-guided punctures were recorded from skin penetration until biopsy needle firing and liver sampling. Thus, the ultrasound punctures contained multiple tissues that occur naturally in the liver biopsy needle route. These data represented a close simulation of the future clinical use of the biopsy needle.

The visually controlled punctures were targeted to one tissue at a time, and the needle location was verified visually. The stomach of the pig was opened for visual control punctures, so that the needle operator could see the organs and was able to control which organ was punctured by the needle. For muscle and fat measurements, the skin was cut to provide a view of the tissues. Adipose tissue was measured from the back of the neck and muscle from hind leg (m. biceps femoris, m. semitendinosus). No tissue desiccation was made, and the punctures were done *in vivo*. Blood circulation was active in all tissues during the punctures of fat, muscle, liver and spleen. Blood measurements were the only exception: Venous blood was collected from ear vein to a vial for the measurement. Blood measurements were performed immediately after blood collection, and old blood was replaced with fresh blood in the vial before blood clotting after two measurements. Each tissue was measured three times using the same needle, but always from a different puncture site. Seven needles were used, resulting in 21 punctures for each tissue type. From each puncture, a time-dependent measurement signal from the forward moving needle was simultaneously recorded from 15 measurement frequencies at a sampling rate of 200 Hz. This resulted in approximately 3 min of data from each tissue type. The biopsy needle was in the loaded state, and variations from normal tissue heterogeneities and from needle movements were present in the data in order to provide as realistic data as possible for our classifier. Time stamps were put into the data when the

BMES BIOMEDICAL ENGINEERING SOCIETY

needle tip was totally in the desired tissue and was moving forward in good contact with the desired tissue. The needle penetrated into the tissue for a couple of centimeters. The data were collected in real time, and thus the signal emerged from the structural inhomogeneties of the tissue during the movements of the needle. One time stamp per puncture was marked to the data. Each puncture was made in a slightly different location. This provided reliable data from a single tissue only.

Analysis of In Vivo Data and Tissue Classifier

Data characteristics were analyzed qualitatively from the whole data set but quantitatively from only the visually controlled biopsy data. In practice, the measurement signal period 0.5 s before until 0.5 s after the time stamp (200 data points) from each measurement was included in the analysis and resulted in approximately 21 seconds of data from each tissue (4200 data points). This ensured that only data with a known origin of the forward moving needle were included in the classifier performance evaluation. Moreover, it standardized the amount of data between tissue types.

The data were manually checked and clearly erroneous looking tissue positions, indicated as outliers and strong noise, were removed. Normal variation due to needle movements and other factors were conserved.

The outliers were removed using the threshold method: values under or over a specified threshold were considered as outliers. The threshold value was manually selected based on the data analysis using histograms and different visualization tools. The threshold value was selected so large that only values that were clearly different from the majority of data of the tissue type in question were identified as outliers. The thresholds in 127 kHz impedance magnitude were $4000\,\Omega < Z < 20{,}000\,\Omega$ included for fat, $0\,\Omega < Z < 4000\,\Omega$ for muscle, $0\,\Omega < Z < 2500\,\Omega$ for blood, and $2000\,\Omega < Z < 5800\,\Omega$ for liver. The amount of data obtained from different tissues are shown in Table 1. Liver data contained more outliers than the other tissue data. The reason for most of the liver outliers was most likely blood. The liver is a well-vascularized organ, and punctures cause bleeding. From fat, there were two punctures more than from other tissues, and therefore fat tissue data were 2 s longer.

The tissue classifier was created based on the original visual-control data, without error correction, measured with the biopsy needle. The performance values of the classifications were calculated using a sevenfold, needle-specific hold-out method. The classifier was created using data from six needles, and the data from the hold-out needle were used as testing data. This was done seven times so that each needle was left out once. The final performance value was averaged over all seven rounds.

The classification model was a statistical model based on the Gaussian distribution and the maximum likelihood principle as in Ref. 7. The likelihood p was the probability of sample vector × to belong to class ω_j, calculated by

$$p\left(x|\omega_j\right) = \frac{1}{(2\pi)^{\frac{d}{2}}|\Sigma_j|^{\frac{1}{2}}} e^{\left[-\frac{1}{2}(x-\mu_j^T)\Sigma_j^{-1}(x-\mu_j)\right]},$$

where μ_j and Σ_j are the mean and covariance of class ω_j, respectively, and d is the number of dimensions in the feature space. The final classification result was the tissue class that had the highest likelihood.

The method finds the best classification result even when the likelihoods are low. However, then the classification may often be incorrect. To avoid this kind of misleading classification result, we have used threshold when classifying the ultrasound guided punctures: If the likelihood is lower than the threshold value 10^{-4} for all of the tissue classes, the data point is classified as 'No Class'.

Measurement data of 30 simultaneous values (magnitude and phase angle of 15 frequencies) were reduced to features calculated from the data in order to reduce dimensionality and provide real-time classification. The features described the DC level and the shape of the impedance magnitude and phase angle

TABLE 1. Data during time stamps of visually controlled punctures were selected for the classifier creation.

	Visual control data		Data from time stamps		Outliers removed		Data for analysis	
	Number of samples	(s)	Number of samples	(s)	Number of samples	(s)	Number of samples	(s)
Fat	52,323	262	4600	23	280	1.4	4320	22
Muscle	42,682	213	4200	21	64	0.3	4136	21
Blood	37,007	185	4200	21	155	0.8	4045	20
Spleen	37,276	186	4200	21	0	0.0	4200	21
Liver	35,017	175	4200	21	554	2.8	3646	18

Clear outliers were removed, and the remaining data were used in analysis and classifier creation. The number of samples is shown both in numbers of samples and in duration (in seconds). One sample comprises 15 impedance magnitudes and 15 phase angles.

spectra. Impedance at higher frequencies were weighted more than lower frequencies to reduce the effect of EII. Based on the feature vector values, the probabilities that the sample belonged in different tissue classes was calculated.

The total accuracy of the classification was defined as all correct classifications/all classifications. Sensitivity was defined for each tissue class as true positive cases/all positive cases and specificity as true negative cases/all negative cases.

RESULTS

Simulations

The sensitivity distribution was focused on the needle facet, and especially on the volume around the tip of the electrode wire (Fig. 4). Over 90% of the sensitivity distribution was within the elliptic cylinder

volume of height 0.5 mm and semi-axis radii of 0.4 mm and 0.6 mm on the needle facet.

The simulated impedance values of the homogeneous materials are shown in Table 2 to present the absolute differences between the materials.

Penetration to another tissue caused an impedance change when the inner electrode contacted the new tissue. Figure 5 shows an example of impedance signals from penetrations from one tissue to another with different tissue sizes and conductivities. The zero point is defined to be at the tissue boundary. The results show that the impedance change was significant when about 0.5 mm of the needle tip was in the new tissue (Table 3). This was to be expected as the measurement needs two electrodes and after 0.5 mm penetration both the electrodes are in contact with the new tissue. Saline measurements in the laboratory have also shown that the very tip of the needle has to be in the saline before changes in impedance occur. When the needle entered the new tissue, the signal followed the
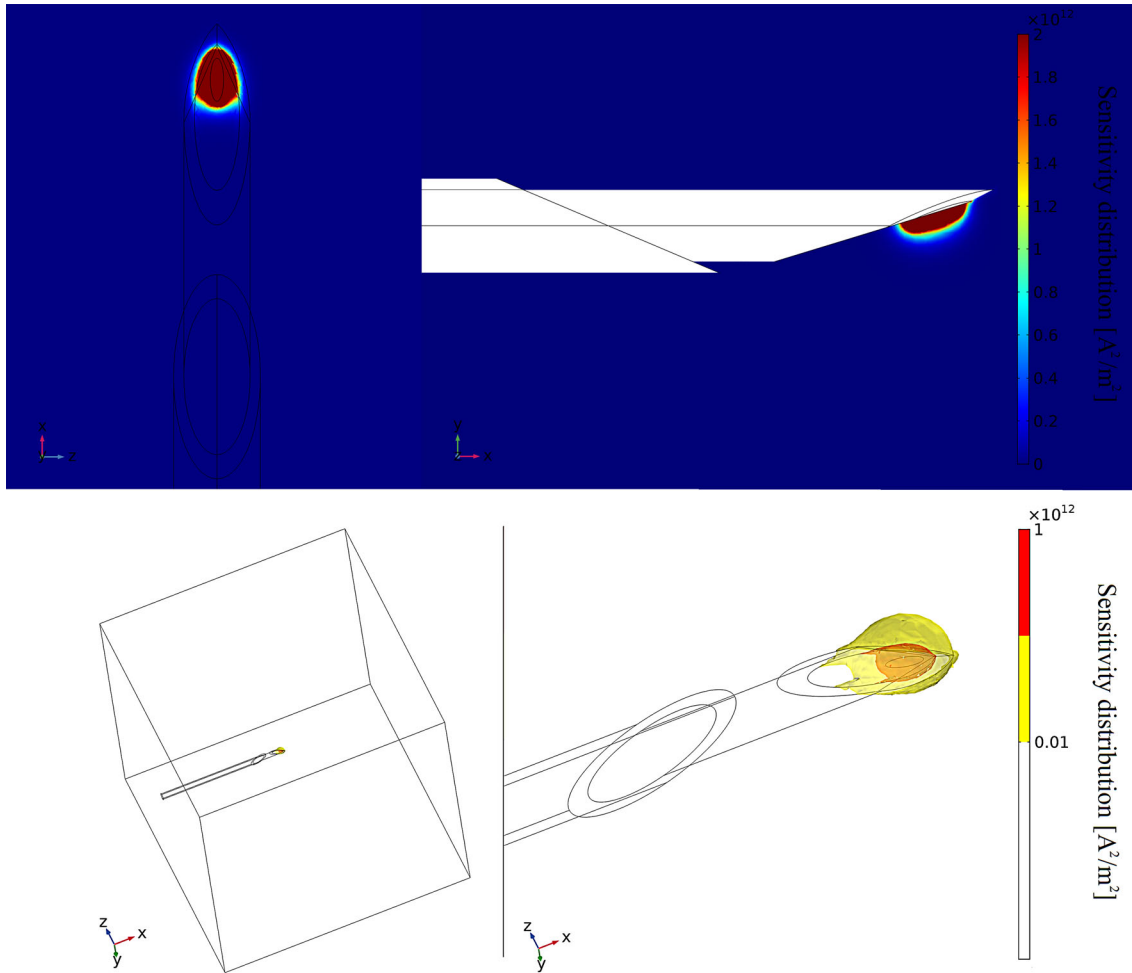

FIGURE 4. Sensitivity distribution of the biopsy needle in the homogeneous volume conductor. Needle is in $50 \times 50 \times 50$ mm^3 cube, outer needle diameter is 1.3 mm.

same path regardless of the size of the new tissue. Hence, the signal and detection points were the same whether the needle totally penetrated new large tissue or just entered a small heterogeneity or membrane (Fig. 5). The signal was not disturbed by the tissues in front of the needle, and the signal was only affected by tissues directly on the facet.

The new tissue was correctly measurable when about 1.2 mm of the needle was in new tissue (Table 3, Fig. 5). Because the length of the biopsy needle facet is over 3 mm, the new tissue was correctly measurable with all simulated conductivity differences before the whole needle facet was in the new tissue. All that was required was that parts of both electrodes were in the new tissue type. The signal curve from the penetration had a sharper shape when penetrating through lower-conducting material than higher-conducting material. Hence, the change in impedance was slightly higher earlier when the new tissue had higher conductivity than the tissue where the needle had previously been (Fig. 5).

Small targets with sizes of $2 \times 2 \times 2$ mm^3 were correctly measurable with all simulated conductivity and relative permittivity values. The length at which the heterogeneity was correctly measurable (Table 3) depended to some extent on conductivity and relative permittivity, but even with the largest differences in conductivity and permittivity, the correct measurement value was achievable at least for a length of 1.1 mm.

When the target was smaller than $1 \times 1 \times 1$ mm^3, the impedance of the target was no longer correctly measurable, but it could be detected because it affected the impedance and the value became a mixture of the surrounding tissue and the target (Fig. 5). When the small target or membrane had passed the electrode wire, impedance recovered, but the effect of heterogeneity was "longer" than the actual thickness of the heterogeneity. Table 4 shows for how long different sizes of heterogeneities affected the measurement va-

FIGURE 5. Example of impedance signals during ▶ penetration through heterogeneities of different sizes and different conductivities. Conductivity σ and relative permittivity ε_r of the heterogeneities are shown in each figure. The surrounding tissue conductivity and permittivity was 0.1 S/m and 5000, respectively. A membrane with a thickness of 1 mm and a small target with a size of $1 \times 1 \times 1$ mm^3 provided almost identical impedance signals (graphs overlap). Grey lines show the impedance magnitude levels of 5% greater/less than the bulk material and 5% less/greater than the inclusion, and corresponding values of 2° in phase angle.

lue. Already, $0.2 \times 1 \times 1$ mm^3 targets caused a detectable change in the impedance when the needle tip penetrated through them (Fig. 5, Table 4). However, $10 \times 10 \times 10$ mm^3 heterogeneities next to, or above or below the needle tip did not affect the impedance. Thus, only objects in front of the path of the needle affected the measured signal. All signals remained at the impedance values of the large block (difference less than 2% in magnitude and less than 2° in phase angle) regardless of the heterogeneity above, below, or beside the needle.

In Vivo Data

Tissue data were measured *in vivo* in a porcine model. As seen from example punctures to the liver (Fig. 6), the raw data had high variation. Short periods also showed the periodic behavior of the signal. This could have been due to the ordered histological structure of the liver, but we were unable to verify the microscopic penetration route.
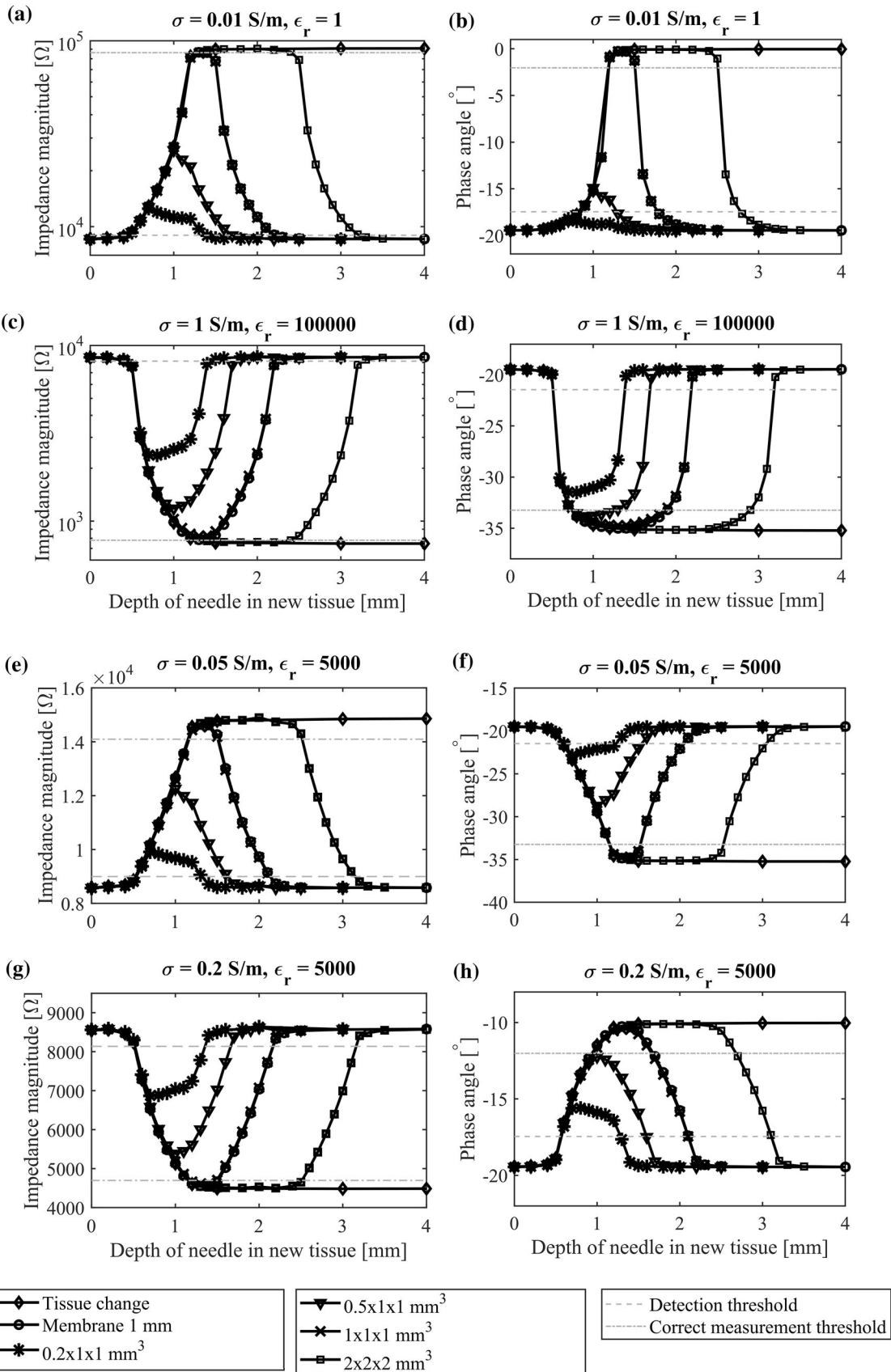
Visual-control data from different tissues *in vivo* are shown in Fig. 7. The values are raw values without measurement error correction. All the measured tissues lie between 1 kΩ and 1 MΩ at 127 kHz. The liver impedance magnitude had median 3330 Ω and quartiles 3154 and 3512 Ω, phase angle median − 23.2°, and quartiles − 24.4° and − 21.9°. When correcting

TABLE 2. Impedance values from computer simulations at 127 kHz.

	Impedance magnitude (Ω)/phase angle (°)				
	Relative permittivity				
Conductivity (S/m)	1	1000	5000	10,000	100,000
0.01	90,838/0	74,189/− 35	24,741/− 74	12,730/− 82	1286/− 89
0.05	18,168/0	17,989/− 8	14,838/− 35	10,495/− 55	1282/− 86
0.075	12,112/0	12,058/− 5	10,957/− 25	8816/− 43	1278/− 84
0.1	9084/0	9061/− 4	8565/− 19	7419/− 35	1273/− 82
0.133	6830/0	6820/− 3	6601/− 15	6032/− 28	1263/− 79
0.2	4542/0	4539/− 2	4473/− 10	4283/− 19	1237/− 74
1	908/0	908/0	908/− 2	906/− 4	742/− 35

(a) $\sigma = 0.01$ S/m, $\epsilon_r = 1$

(b) $\sigma = 0.01$ S/m, $\epsilon_r = 1$

(c) $\sigma = 1$ S/m, $\epsilon_r = 100000$

(d) $\sigma = 1$ S/m, $\epsilon_r = 100000$

(e) $\sigma = 0.05$ S/m, $\epsilon_r = 5000$

(f) $\sigma = 0.05$ S/m, $\epsilon_r = 5000$

(g) $\sigma = 0.2$ S/m, $\epsilon_r = 5000$

(h) $\sigma = 0.2$ S/m, $\epsilon_r = 5000$

Impedance magnitude [Ω]
Phase angle [$^\circ$]
Depth of needle in new tissue [mm]

Legend:
- Tissue change
- Membrane 1 mm
- 0.2x1x1 mm^3
- 0.5x1x1 mm^3
- 1x1x1 mm^3
- 2x2x2 mm^3
- Detection threshold
- Correct measurement threshold

BMES BIOMEDICAL ENGINEERING SOCIETY

TABLE 3. Detection and correct measurement depths in different conductivity and permittivity.

Detection depth (mm)/correct measurement depth (mm)/length of correct measurement (mm)

	Relative permittivity				
Conductivity (S/m)	1	1000	5000	10,000	100,000
0.01	0.5/1.3/1.1	0.5/1.3/1.1	0.5/1.3/1.1	0.5/1.3/1.1	0.5/1.3/1.1
0.05	0.6/1.2/1.3	0.6/1.2/1.3	0.6/1.2/1.3	0.5/1.2/1.2	0.5/1.3/1.1
0.075	0.6/1.2/1.3	0.6/1.2/1.3	0.7/1.1/1.4	0.6/1.2/1.3	0.5/1.3/1.1
0.1	0.6/1.2/1.3	0.6/1.2/1.3	NA/NA/NA	0.6/1.1/1.4	0.5/1.3/1.1
0.133	0.6/1.2/1.3	0.6/1.2/1.4	0.6/1.1/1.4	0.6/1.1/1.4	0.5/1.3/1.1
0.2	0.6/1.2/1.3	0.6/1.2/1.3	0.6/1.2/1.3	0.6/1.2/1.3	0.5/1.3/1.1
1	0.5/1.3/1.1	0.5/1.3/1.1	0.5/1.3/1.1	0.5/1.3/1.1	0.5/1.3/1.1

'Detection depth' from the tissue boundary—the distance from the new target tissue boundary when the needle signal deviates due to the vicinity of the boundary more than the selected noise level. 'Correct measurement depth' shows the needle depth in new tissue when the impedance signal of the target tissue was achieved within the noise level. 'Length of correct measuement' is the largest length of correct measurement with $2 \times 2 \times 2$ mm^3 target. It is defined from the "first correct measurement depth" until the "last correct measurement depth" when the needle is passing through a target tissue of $2 \times 2 \times 2$ mm^3.
NA not applicable.

TABLE 4. Interval of depth points (mm) when there was a significant effect of the heterogeneity on the impedance signal.

		Size of the heterogeneity (mm^3)				
Conductivity (S/m)	Relative permittivity	$2 \times 2 \times 2$	$1 \times 1 \times 1$	$0.5 \times 1 \times 1$	$0.2 \times 1 \times 1$	$25 \times 50 \times 50$
0.01	5000	0.5–3.1	0.5–2.1	0.5–1.6	0.5–1.3	0.5–
0.05	5000	0.6–3.1	0.6–2.1	0.6–1.6	0.6–1.3	0.6–
0.075	5000	0.7–3.0	0.7–2.0	0.7–1.5	0.7–1.2	0.6–
0.133	5000	0.6–3.0	0.6–2.0	0.6–1.5	0.7–1.2	0.6–
0.2	5000	0.6–3.1	0.6–2.1	0.6–1.6	0.6–1.3	0.6–
1	5000	0.5–3.2	0.5–2.2	0.5–1.7	0.5–1.4	0.5–
0.1	1	0.6–3.1	0.6–2.1	0.6–1.6	0.6–1.3	0.6–
0.1	1000	0.6–3.0	0.6–2.0	0.6–1.5	0.6–1.2	0.6–
0.1	10,000	0.6–3.1	0.6–2.1	0.6–1.6	0.6–1.3	0.6–
0.1	100,000	0.5–3.2	0.5–2.2	0.5–1.7	0.5–1.4	0.5–

The tissue boundary is at 0 mm. A membrane with a thickness of 1 mm provided basically the same results as a $1 \times 1 \times 1$ mm^3 target, and therefore the membrane is not included in the table.

the measurement device error based on the RC component model and compensating for the stray capacitance, the liver impedance median was 2950 Ω and $- 60°$.

The parameters derived from the impedance measurements from different tissue types formed separate but partially overlapping clusters. Figure 7 shows the relationship of the tissue impedance values to each other in the impedance magnitude and phase angle space. Fat has low conductivity, and therefore had the highest impedance. Blood has high conductivity and the lowest impedance. Liver has characteristics between those of the spleen and muscle. Depending on tissue type, differentiation from other tissues varied. However, not even fat can be reliably differentiated from other tissues based on single frequency magnitude alone.

Tissue Classifications

Classification results based on the needle-specific hold-out method are shown in Table 5. The total accuracy (all correct classifications/all classifications) was approximately 94%. Fat was the most accurately classified tissue. Because muscle, spleen, and liver tissues are similar, they yielded more misclassifications. Still, their classification accuracies were over 90%.

The sensitivity to classify certain tissue is shown in the diagonal values of Table 5 (e.g. 'Liver', 91%, 'Fat' is 99%). Specificities for 'Liver', 'Spleen', 'Blood', 'Muscle' and 'Fat' are 97, 99, 100, 96 and 100%.

An example of ultrasound-guided liver biopsy punctures is shown in Fig. 8. Raw data had high variation, yet classification could be performed, and the device mostly knew correctly where the needle tip was during the puncture.
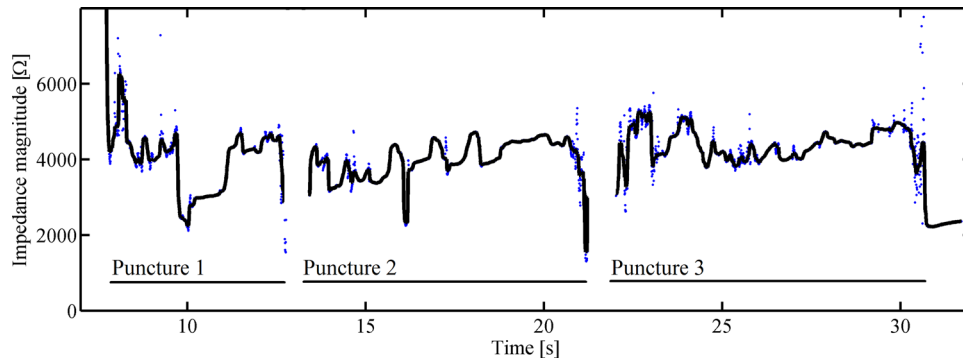
FIGURE 6. Example data of punctures to the liver with the biopsy needle. The figure contains three punctures to different locations with a single needle. Data are from the moving needle. Only one frequency plotted. Median-filtered data are shown in black, and raw data points are shown in blue.
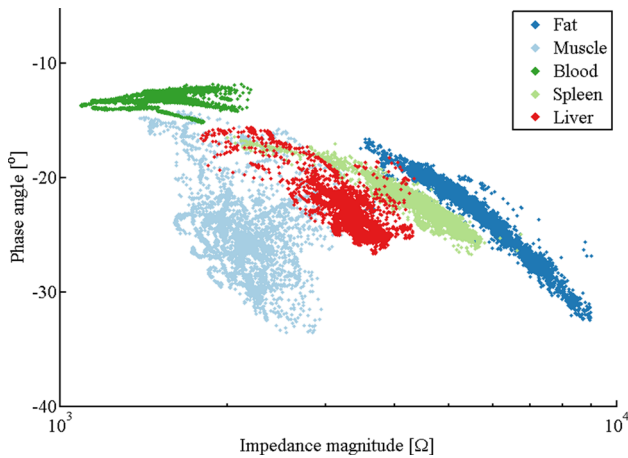

FIGURE 7. *In vivo* tissue data at 127 kHz. Needle location verified by visual control. Measurement values are raw values without error correction.

DISCUSSION

Measurement Resolution

In biopsy applications, an optimal sensitivity field should enable the detection of a tumor in the path from where the biopsy will be taken. Thus, this depends not only on the requirements to detect tumors of various sizes, but also when a tumor is detected then the tool should capture some tumorous tissue. A large sensitivity volume would also mean a large lateral sensitivity area. Thus, the needle would also be sensitive to tissue changes that are not actually in the path of the needle, which provides misleading guidance. Hence, we believe that our impedance measurement configuration with a small measurement volume at the front of the needle would produce better tissue assessment for the biopsy. The computer simulations show that the measurement sensitivity distribution of the IQ-Biopsy needle is focused on the very tip of the needle and spatially offers very precise tissue identification. The simulations also show that tissue structures next to the needle do not cause artifacts in the measurement values. Thus, the target at the front of the tip that is measured will always also be sampled in a biopsy.

According to our simulations, the correct impedance measurement of the target is already achievable when part of the needle tip is in new tissue. The resolution of the method is high, and even $2 \times 2 \times 2$ mm^3 targets at the front of the tip are correctly measured with the device. Results in Table 3 also demonstrate that the conductance and relative permittivity of the surrounding tissue do not have a major impact on measurement resolution. Furthermore, even much smaller targets are easily detected by changes in impedance. Thus, in homogeneous tissue with a variation of less than 5%, the method could theoretically detect small tumors or malignancies even if their electrical properties differ only slightly from the surrounding tissues (for example, surrounding conductivity 0.10 S/m, target 0.13 S/m). In practice, the signal varies due to electrical measurement noise, differences between individuals, and the inhomogeneity of the tissue, and thus tumor detection is made more challenging. The use of multiple frequencies, however, can increase detectability despite this variation.

High resolution is a desired property, but highly local sensitivity distribution may cause large variations in the signal, since even small heterogeneities at the needle tip affect the impedance. We saw this in both simulations and *in vivo* data; even 0.2 mm thin targets affected the signal value in the simulations if they were exactly at the needle tip. *In vivo* porcine data, verified visually being from single tissues, show high variation in the raw measurement values. Even in macroscopically homogeneous tissue, the measurement signal varies due to tissue structures. For example, the liver is composed of hexagonal lobules with blood vessels in the middle and in the vertices and connective tissue

BMES BIOMEDICAL ENGINEERING SOCIETY

TABLE 5. Measurement-based classification results in different needle locations.

	Needle location, verified visually				
	Fat	Muscle	Blood	Spleen	Liver
Classification					
Fat	99%	0%	0%	0%	0%
Muscle	0%	93%	8%	2%	5%
Blood	0%	0%	92%	0%	0%
Spleen	0%	1%	0%	94%	4%
Liver	0%	6%	0%	4%	91%
Amount of data	432,0 22 s	413,6 21 s	404,5 20 s	420,0 21 s	364,6 18 s

The amount of data is shown both in the number of data samples and in seconds. One data sample comprises 15 impedance magnitudes and phase angles.
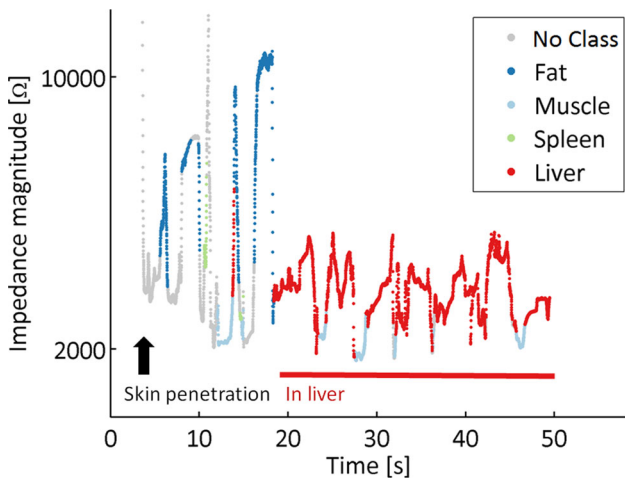
FIGURE 8. Single-frequency impedance magnitude raw signal during one ultrasound-guided liver biopsy. The red line indicates the ultrasound tissue identification. Coloring of the signal curve is according to the classification based on full spectral analysis. The classification model was created using the visual-control data.

between the lobules. However, the *in vivo* measured data provided excellent tissue identification results. Therefore, based on our results, the spatial sensitivity of the needle is excellent for the purpose of biopsies.

The clinically popular ultrasound-guided liver punctures could benefit from highly local measurement because the resolution of ultrasonography is limited and identifying the very tip of the needle on an ultrasound image is challenging. Bioimpedance-based tissue identification could provide precise real-time location for tissue sampling. On the other hand, our needle system could also benefit from ultrasound imaging to guide the needle close to the target, as our needle only senses the very local tissue at the needle tip. In addition, core biopsy needles shoot approximately 2 cm forward and collect not only very local tissue, but also material further away that the needle can measure.

Measurement Value Accuracy

There is discrepancy between measured and simulated spectra especially in low frequencies as seen in Fig. 2. Electrode interface impedance (EII) is one major explaining factor for the difference as in our simulations we omitted the complex electrode interface as its effect depend on electrode material and the tissue electrolytic properties and on the amplifier characteristics. However this has profound effect as the needle system used two electrode measurement setup. Moreover in real measurements instrumentation, cabling, stray capacitance of cabling *etc.*, have an effect. All these contribute to the observed large difference of the impedance magnitude in low frequency compared to simulations. The difference in high frequencies is much smaller, however still these factors may deviate the measured values. For example in 0.9% saline solution, the measured impedance at room temperature (22 °C) at a frequency of 127 kHz with IQ-Biopsy was 760 Ω (2STD: 650, 870 Ω) with phase of − 13.5° (− 11.3, − 15.7) (capacitance of cabling is compensated). Simulations with conductivity of 1.3 S/m and relative permittivity of 80 suggest that impedance should be 700 Ω and 0°. Thus, the measured impedance magnitude is about 60 Ω too high at 127 kHz in saline and phase angle is 13.5° too low. In tissues, the effect of EII and measurement error may behave in different way than in saline.

We reported the impedance values of five tissues at 127 kHz measured *in vivo* from the living animal. At this frequency range, EII is not such a major issue as it is in saline measurements at low frequencies. The measured median impedance value of liver at 127 kHz corresponded to the simulated impedance with a conductivity of approximately 0.16 S/m and a relative permittivity of approximately 38,000.

In the literature, the reported conductivity values at 100 to 127 kHz vary between 0.09 and 0.25 S/m, and the relative permittivity values vary between 6000 and 40,000.[4,6,19,23–25,28] The ranges of liver material properties found in the literature were used in the simula-

TABLE 6. Comparison of measured and simulated impedance of liver.

Impedance magnitude (Ω)/phase angle (°)						
Measured liver			Simulated liver			
Median	Conductivity (S/m)	0.09	0.09	0.15	0.25	0.25
	Relative permittivity	8000	40,000	40,000	8000	40,000
2950/− 60		9020/− 32	3230/− 72	3000/− 62	3740/− 13	2540/ 49

Simulations cover the wide range of conductivities and permittivities of liver reported in the literature.

tions, and the resultant impedances are shown in Table 6 together with the measured impedance values. As shown in Table 6, impedances in our measurements are within the range that was obtained in simulations with material properties taken from the literature. However, the conductivities may not be directly comparable to the macroscopic conductivities presented in the literature because the measurement setup, instrumentation, and sub-needle-tip size sensitivity distribution make comparisons difficult. Further, most of the data available in the literature are post-mortem data from tissue samples. Our data, however, provide electrical material property values from living tissues.

A tetrapolar configuration would, in theory, provide more accurate impedance values as the effects of EII would be diminished. However, a tetrapolar measurement system, in addition to being considerable more complex to realize in a needle tip, would create a new source of uncertainty due to its even smaller and very complex sensitivity distribution with volumes of negative and positive sensitivities shown in impedance cardiography,[16] EIT,[17] and microelectrode environments.[3] For needle guidance, this would be a major problem when interpreting the results taking into account the complex sensitivity distribution and the inhomogeneous real tissue volume conductivity shown here. Therefore, we consider that for biopsy guidance, the bipolar configuration of the needle can be considered to be a good compromise.

The depth of the needle could in theory effect the impedance measurements, as in our case the entire needle body acts as another electrode. This has been shown to be the case in needle measurements with an electrode configuration, where the measurements is done between the needle and the surface electrode. In our case, because the electrodes are so very close to each other, the major part of the current flows in the small area at the needle facet, and the depth of the needle shaft does not have significant impact on the measurement. In addition to theoretical considerations, this has also been tested in laboratory tests with saline. No significant effect has been noted from the depth of needle shaft entering the measured volume (data not shown).

Tissue Discrimination and Classification

Tissue heterogeneities are a challenge for tissue classification creation since the created model should tolerate normal variation during the movement of the needle in tissue. Due to the variations, comprehensive training data are important. In this study, the impedance data were gathered from different tissues *in vivo*. The use of living tissue, multiple needles, multiple puncture sites, and moving needles are clear strengths of this study.

We acknowledge that the gathered tissue data originates from a single individual. Because impedance can vary between individuals, inter-subject variation has the potential to alter the classification performance. However, variation is also high within the same tissue type in a single individual as we have shown here. Different tissue heterogeneities and different measurement locations produced large variations in measured impedance. Thus, in our case, when the measurement is performed from the small volume at the front of the needle facet, it is likely that the variation within the subject is already highly representative. Moreover, the variation between subjects is most probably relatively smaller compared with the effect of tissue heterogeneity within each subject.

Based on the needle measurements, a tissue classifier capable of differentiating fat, muscle, blood, spleen, and liver was created. Tissue discrimination performance was good, approximately 94% total accuracy was achieved. Fat and blood, for example, have different conductive properties already, but muscle, spleen, and liver are more alike in their electrical properties. The differentiation of liver, spleen, and muscle from each other shows that our classifier can also discriminate tissues with less obvious impedance differences. However, using only one frequency magnitude, reliable differentiation is not possible since multiple tissue types overlap each other.

The exact needle location information in this study was limited to the macroscopic tissue information available either visually or by ultrasonography. The classification performance values were calculated using data from the time periods during time-stamps which

indicated proper needle contact with the desired tissue and forward needle procession. The whole data set from needle penetrations was also analyzed qualitatively, but reliable quantitative analysis requires data that are measured reliably from the desired tissue type.

Heterogeneities in tissue occasionally affected the classification in dynamic measurement. For example, when the needle stopped or was withdrawn from tissue, the impedance values represented blood. We can hypothesize that in these circumstances, blood or extracellular fluid accumulated around the needle tip and changed the measurement value. According to the simulations, 0.2 mm thick heterogeneity with 1 S/m conductivity can decrease the impedance of 0.1 S/m conducting tissue by approximately 70%. Another example is the measurement signal from liver, which seemed to have some periodic characteristics when the needle was penetrating into the tissue. This might have been due to the liver's repetitive structure, including hexagonal lobules with blood vessels. However, periodicity was not always present, and because the needle penetration velocity was not constant, and the penetration angle not fixed, structure thicknesses and their effects on the signal cannot be verified. In real tissues, needle velocity is difficult to standardize, since even though the needle is moved at a constant speed, the needle tip speed inside the tissue with respect to the tissue can change due to differences in tissue stiffness, membrane structures, *etc*. Constant needle velocity is therefore not possible in studies of *in vivo* and is also irrelevant for clinical use.

Because the sensitivity distribution is so focused on the needle tip, even small heterogeneities or small amounts of fluid can change the measurement values. Thus, with the small measurement volume, as we have shown, the small inhomogeneities in every tissue produced by, e.g., blood vessels, pockets of stroma, and liver lobules, all have an effect on the impedance signal, and thus have an impact on classification accuracy. However, as our results have shown, the classification can still be obtained with good accuracy. In the example case study in Fig. 8, for example, when the needle is in liver, the classification is correct 86% of the time. There were also misclassifications, such as muscle (11% of time), but most of those occasions were short, and it may be possible to remove them using signal processing.

If other electrode configurations are used that produce large sensitivity volumes, the measurements may not only fail to reflect purely small target tissues at the needle tip but will also include the surrounding tissues,[9] and thus identification of the volume at the front of the needle could be compromised.

The speed of the penetration could compromise the tissue identification accuracy. The sampling rate and classification rate of our measurement device was 200 Hz, and thus we measured all 15 frequencies and also classified the measured tissue with each 5 ms. Based on the simulations, most of our sensitivity is within the volume of 0.5 mm height and a 0.4 × 0.6 semi-axis radius cylinder. We can assume that to be able to measure the needle penetration route, at least two measurements per every cylinder are needed. This can be achieved if the penetration speed is 10 cm/s or less. This theoretical maximum penetration speed is fast, and not considered realistic during a normal biopsy. Therefore, within typical ranges, the penetration speed most likely does not affect classification accuracy.

The main source of the variation is most likely the tissue heterogeneity. When used in clinical practice, possible tissue misclassifications as blood during withdrawal of the needle are easily interpretable by physicians who move the needle and know when they are withdrawing or stopping the needle. Therefore, brief misclassifications, especially during needle withdrawal, are not considered to be critical drawbacks.

The tissue classification performance reported here provides preliminary results of tissue identification. Tissue identification performance may differ when the device is used in a clinical setting and tumour differentiation is still a question that needs to be answered in future clinical studies. However, we consider that our *in vivo* study using a pig model provides realistic data and represents well the clinical case in the sense of noise and tissue heterogeneity. It does not provide tumor data, as no large animal tumor model was available. However, liver and spleen have limited contrast between each other in terms of conductivity (at 127 kHz liver 0.09 S/m and spleen 0.12 S/m[1]). Therefore, because organs such as the spleen and liver can be separated, perhaps other not-so-evidently different tissues, such as tumors, could also be differentiated with the device.

In addition to the potential to help with selecting the proper site to take a biopsy, the impedance data could also provide information on the tissues in the path of the needle prior to the biopsy. This could be clinically important, for example, to provide a better view of the extent of cancer.

CONCLUSIONS

To conclude, the results of this study show that during biopsy needle puncture, tissues can be accurately identified *in vivo* and in real-time using bioimpedance needle measurement with a highly targeted electrode arrangement. The simulations in this study showed that the needle tissue detection is spatially very accurate and new tissues with a size of 2 × 2 × 2 mm^3

can be accurately measured, and even 0.2 mm thick small tissue patches can be identified. Due to the high spatial sampling, tissue heterogeneities cause variations in the local bioimpedance measurement of the needle system. However, the classifiers were able to overcome this problem, and good results were achieved in identifying five separate tissue types in this preliminary study with one subject. Thus, the spatial accuracy of the needle system presented in this study indicates to be well suited for biopsy. Overall, the IQ-Biopsy needle and the tissue identification method are expected to have high potential to improve biopsy quality.

CONFLICT OF INTEREST

SH, JK, PA, KK are employees of Injeq and have patents pending about the Injeq IQ-Biopsy. SH, JK, PA hold options, PA, KK, JH are shareholders, KK, JH are co-founders, and JH is a board member of Injeq.

REFERENCES

[1]Andreuccetti, D., R. Fossi and C. Petrucci. An Internet resource for the calculation of the dielectric properties of body tissues in the frequency range 10 Hz - 100 GHz. IFAC-CNR, Florence (Italy), 1997. Based on data published by C. Gabriel et al. in 1996. http://niremf.ifac.cnr.it/tissprop/. Accessed 3 July 2017.

[2]Annus, P., R. Land, M. Min, M. Reidla, and M. Rist. Notes on applicability of the impedance spectroscopy for characterization of materials and substances. Instrumentation and Measurement Technology Conference Proceedings (I2MTC), 2016 IEEE International, pp. 1–6.

[3]Böttrich, M., J. M. A. Tanskanen, and J. A. K. Hyttinen. Lead field theory provides a powerful tool for designing microelectrode array impedance measurements for biological cell detection and observation. *Biomed. Eng. Online* 16(1):85, 2017.

[4]Gabriel, S., R. W. Lau, and C. Gabriel. The dielectric properties of biological tissues: II. Measurements in the frequency range 10 Hz to 20 GHz. *Phys. Med. Biol.* 41:2251–2269, 1996.

[5]Geselowitz, D. B. An application of electrocardiographic lead theory to impedance plethysmography. *IEEE Trans. Bio-Med. Eng.* 18:38–41, 1971.

[6]Haemmerich, D., S. T. Staelin, J. Z. Tsai, S. Tungjitkusolmun, D. M. Mahvi, and J. G. Webster. In vivo electrical conductivity of hepatic tumours. *Physiol. Meas.* 24(2):251–260, 2003.

[7]Halonen, S., K. Annala, J. Kari, S. Jokinen, A. Lumme, K. Kronström, and A. Yli-Hankala. Detection of spine structures with Bioimpedance Probe (BIP) Needle in clinical lumbar punctures. *J. Clin. Monit. Comput.* 31(5):1065–1072, 2017.

[8]Halonen, S., E. Kankaanpää, J. Kari, P. Parmanne, H. Relas, K. Kronström, R. Luosujärvi, and R. Peltomaa. Synovial fluid detection in intra-articular injections using Bioimpedance Probe (BIP) Needle—a clinical study. *Clin. Rheumatol.* 36:1349–1355, 2017.

[9]Halonen, S., J. Kari, P. Ahonen, T. Elomaa, P. Annus, and K. Kronstrom. Biopsy needle including bioimpedance probe with optimized sensitivity distribution. *Int. J. Bioelectromagn.* 17(1):26–30, 2015.

[10]Halter, R. J., A. Schned, J. Heaney, A. Hartov, S. Schutz, and K. D. Paulsen. Electrical impedance spectroscopy of benign and malignant prostatic tissues. *J. Urol.* 179(4):1580–1586, 2008.

[11]Hernandez, D. J., V. A. Sinkov, W. W. Roberts, M. E. Allaf, A. Patriciu, T. W. Jarrett, L. R. Kavoussi, and D. Stoianovici. Measurement of bio-impedance with a smart needle to confirm percutaneous kidney access. *J. Urol.* 166(4):1520–1523, 2001.

[12]Kalvøy, H., L. Frich, S. Grimnes, Ø. G. Martinsen, P. K. Hol, and A. Stubhaug. Impedance-based tissue discrimination for needle guidance. *Physiol. Meas.* 30(2):129–140, 2009.

[13]Kalvøy, H., and A. R. Sauter. Detection of intraneural needle-placement with multiple frequency bioimpedance monitoring: a novel method. *J. Clin. Monit. Comput.* 30(2):185–192, 2016.

[14]Kari J., K. Annala, P. Annus, V.-P. Seppä, and K. Kronström. A thin needle with bio-impedance measuring probe: tissue recognition performance assessed in in vivo animal study, 2015. https://injeq.com/wp-content/uploads/2016/02/BRC-3.1-Kari-et-al.-2015-A-thin-needle-with-bio-impedance-measuring-probe-tissue-recognition-performance-assessed-in-in-vivo-animal-study.pdf. Accessed 30 Oct 2017.

[15]Kauppinen, P. K., J. A. Hyttinen, T. Kööbi, and J. A. Malmivuo. Lead field theoretical approach in bioimpedance measurements: towards more controlled measurement sensitivity. *Ann. N.Y. Acad. Sci.* 873(1):135–142, 1999.

[16]Kauppinen, P. K., J. A. Hyttinen, and J. A. Malmivuo. Sensitivity distributions of impedance cardiography using band and spot electrodes analyzed by a three-dimensional computer model. *Ann. Biomed. Eng.* 26(4):694–702, 1998.

[17]Kauppinen, P. K., J. A. Hyttinen, and J. A. Malmivuo. Sensitivity distribution visualizations of impedance

tomography measurement strategies. *Int. J. Bioelectro-magn.* 8(1):1–9, 2006.

[18]Kwon, H., S. B. Rutkove, and B. Sanchez. Recording characteristics of electrical impedance myography needle electrodes. *Physiol. Meas.* 38(9):1748–1765, 2017.

[19]Laufer, S., A. Ivorra, V. E. Reuter, B. Rubinsky, and S. B. Solomon. Electrical impedance characterization of normal and cancerous human hepatic tissue. *Physiol. Meas.* 31(7):995–1009, 2010.

[20]Lee, B. R., W. W. Roberts, D. G. Smith, H. W. Ko, J. I. Epstein, K. Lecksell, and A. W. Partin. Bioimpedance: novel use of a minimally invasive technique for cancer localization in the intact prostate. *Prostate* 39:213–218, 1999.

[21]Mishra, V., A. R. Schned, A. Hartov, J. A. Heaney, J. Seigne, and R. J. Halter. Electrical property sensing biopsy needle for prostate cancer detection. *Prostate* 73(15):1603–1613, 2013.

[22]Okadana, K., and T. Sekino. Agilent Technologies Impedance Measurement Handbook. Santa Clara: Agilent Technologies Co. Ltd., 2003.

[23]Prakash, S., M. P. Karnes, E. K. Sequin, J. D. West, C. L. Hitchcock, S. D. Nichols, M. Bloomston, S. R. Abdel-Misih, C. R. Schmidt, E. W. Martin, Jr, S. P. Provoski, and V. V. Subramaniam. Ex vivo electrical impedance measurements on excised hepatic tissue from human patients with metastatic colorectal cancer. *Physiol. Meas.* 36(2):315–328, 2015.

[24]Raicu, V., T. Saibara, and A. Irimajiri. Dielectric properties of rat liver in vivo: a non-invasive approach using an open-ended coaxial probe at audio/radio frequencies. *Phys. Med. Biol.* 47:325–332, 1998.

[25]Smith, S. R., K. R. Foster, and G. L. Wolf. Dielectric properties of VX-2 carcinoma versus normal liver tissue. *IEEE Trans. Bio-Med. Eng.* 5:522–524, 1986.

[26]Sonn, G. A., S. Natarajan, D. J. Margolis, M. MacAiran, P. Lieu, J. Huang, F. J. Dorey, and L. S. Marks. Targeted biopsy in the detection of prostate cancer using an office based magnetic resonance ultrasound fusion device. *J. Urol.* 189(1):86–92, 2013.

[27]Trebbels, D., F. Fellhauer, M. Jugl, G. Haimerl, M. Min, and R. Zengerle. Online tissue discrimination for transcutaneous needle guidance applications using broadband impedance spectroscopy. *IEEE Trans. Bio-Med. Eng.* 59(2):494–503, 2012.

[28]Wang, H., Y. He, M. Yang, Q. Yan, F. You, F. Fu, T. Wang, X. Huo, X. Dong, and X. Shi. Dielectric properties of human liver from 10Hz to 100MHz: normal liver, hepatocellular carcinoma, hepatic fibrosis and liver hemangioma. *Bio-Med. Mater. Eng.* 24(6):2725–2732, 2014.

[29]Wolf, M., R. Gulich, P. Lunkenheimer, and A. Loidl. Broadband dielectric spectroscopy on human blood. *Biochim. Biophys. Acta. BBA* 1810(8):727–740, 2011.